HHS Public Access

Author manuscript

Magn Reson Med. Author manuscript; available in PMC 2019 March 01.

Published in final edited form as:

Magn Reson Med. 2018 March ; 79(3): 1429–1438. doi:10.1002/mrm.26801.

Correlation distance dependence of the resonance frequency of intermolecular zero quantum coherences and its implication for MR thermometry

Le Zhang[1,3], **Andrew McCallister**[2,3], **Karl M. Koshlap**[4], and **Rosa Tamara Branca**[2,3,*]

[1]Department of Applied Physical Sciences, University of North Carolina at Chapel Hill, Chapel Hill, NC 27599, US

[2]Department of Physics and Astronomy, University of North Carolina at Chapel Hill, Chapel Hill, NC 27599, US

[3]Biomedical Research Imaging Center, University of North Carolina at Chapel Hill, Chapel Hill, NC 27599, US

[4]Eshelman School of Pharmacy, University of North Carolina at Chapel Hill, Chapel Hill, NC 27599, US

Abstract

Purpose—Since the resonance frequency of water-fat intermolecular zero quantum coherences (iZQCs) can reflect the water-fat frequency separation at the microscopic scale, these frequencies have been proposed and used as a mean to obtain more accurate temperature information. The purpose of this work was to investigate the dependence of the water-fat iZQC resonance frequency on sample structure and on the specific choice of the correlation distance.

Methods—The effect of water-fat susceptibility gradients on the water-methylene iZQC resonance frequency was first computed and then measured for different water-fat emulsions and for a mixture of porcine muscle and fat. Similar measurements were also performed for mixed heteronuclear spin systems.

Results—A strong dependence of the iZQC resonance frequency on the sample microstructure and on the specific choice of the correlation distance was found for spin systems like water and fat that do not mix, but not for spin systems that mix at the molecular level.

Conclusion—Since water and fat spins do not mix at the molecular level, the water-fat iZQC resonance frequency and its temperature coefficient are not only affected by sample microstructure but also by the specific choice of the correlation distance.

Keywords

Intermolecular zero-quantum coherence; MR thermometry; ^{129}Xe

*Correspondence to: Rosa Tamara Branca, Ph.D.: Department of Physics and Astronomy, University of North Carolina at Chapel Hill, Chapel Hill, NC 27599, USA. rtbranca@unc.edu.

INTRODUCTION

The proton resonance frequency (PRF) method has become one of the most widely used methods for MR thermometry thanks to the large, linear temperature dependence of the water resonance frequency (−0.01 ppm/°C) which, in vivo, is virtually independent of tissue types (1). A number of factors have been known to undermine the accuracy of PRF-based thermometry methods, such as macroscopic magnetic field inhomogeneities, motion and field drift (2). Several approaches have been devised to correct for these effects through the use of an internal, temperature-independent reference. In tissues where lipid protons are present, for example, the almost-temperature-independent (3) resonance frequency of the methylene protons is typically used as an internal reference (4). By using the methylene resonance frequency as a reference, the correction of the water resonance frequency can then be done on a voxel scale, either by using spectroscopy-based methods (5–8), by examining the phase change between images acquired at different temperatures (9,10), or by using chemical-shift-based, water-fat separation methods (11,12), which generally allow for a considerable reduction of voxel size.

In order to remove macroscopic field inhomogeneities at a scale much smaller than the resolution achievable with common MRI techniques, people sought to use the signal generated from intermolecular multiple-quantum coherences (iMQCs) (13–15). The iMQC signal is generated by exceedingly small long-range dipolar interactions among spins that reside in different molecules (16) and, sometimes, even in different compartments (17,18). In the past, these signals have been used for a wide range of imaging and spectroscopy applications, which include contrast enhancement in MRI experiments (19–23), and suppression of temporal (24) and spatial inhomogeneities (13,25,26). The removal of macroscopic field inhomogeneities via iMQCs is typically accomplished by the selection of a specific order of coherence, the intermolecular zero quantum coherences (iZQCs), even though, in general, with the proper design of the pulse sequence any other coherence can be used for such a purpose (27–30).

One of the prominent features of iZQC is that its signal naturally evolves at the resonance frequency difference between the two correlated spins. This property alone would not reduce the effect of magnetic field inhomogeneities that exists within a voxel, if it were not for the fact that the bulk of the iZQC signal actually originates from spins that are a “correlation distance” apart. The correlation distance is a “user-controlled” parameter that can be changed by simply altering the strength of the magnetic field gradient pulses used for coherence pathway selection. This distance defines the average distance between the correlated spins from which most of the iZQC signal comes from, and it can be selected to be as large as a few millimeters or as small as few hundreds of micrometers, at which point the magnetic field inhomogeneity or susceptibility gradients present on a larger scale are effectively removed. This property of iZQCs, and specifically the signal generated by water-methylene iZQC coherences has been employed to enhance the accuracy of PRF thermometry (31,32), or as an attempt to measure absolute temperature in fatty tissues (33–35).

However, water and fat spins do not mix and typically reside in different tissue/cell compartments. In addition, water and fat have different magnetic susceptibilities. This means that microscopic susceptibility gradients that are always present at water-fat interfaces on a scale comparable to the correlation distance cannot be completely removed. In this paper, we analyze how susceptibility gradients affect the water-methylene iZQC resonance frequency and discuss the conditions under which the susceptibility gradients dependence of the iZQC resonance frequency is eliminated.

METHODS

Simulations

The iZQC signal arises from multiple quantum operators in the equilibrium density matrix and corresponds to simultaneous "flipping" of correlated spins in opposite directions. Therefore, the iZQC frequency is a reflection of the resonance frequency difference between the correlated spins. To understand the origin and the dependence of the iZQC signal intensity and frequency on sample microstructure and on the correlation distance, we can resort to the quantum picture of iMQCs. Briefly, following a similar derivation described in (16,36), the magnitude of the zero-quantum coherence signal from two spins i and j produced by the prototype iZQC sequence sketched in Figure 1(a) for a spherical sample can be written as:

$$S_{ij}=\frac{3\beta\hbar\omega_0}{8}\tau D_{ij}\ cos(\gamma GTr_{ij}\ cos\,\theta_{ij}), \quad [1]$$

where $\beta=1/k_BT$, ω_0 is the Larmor frequency, G and T are the strength and duration of the correlation gradient which modulates the magnetization and determines the length of the correlation distance d_c as $d_c=\pi/\gamma GT$, θ_{ij} is the angle between the internuclear vector $\vec{r}_{ij}$ and the external field $\overrightarrow{B_0}$ (assumed here to be along the z axis), and D_{ij} is a term that reflects the strength of the dipolar field interaction between the two spins:

$$D_{ij}=(\mu_0/4\pi)\left[3\cos^2\theta_{ij}-1\right]|r|_{ij}^{-3}(\hbar\gamma^2)/4. \quad [2]$$

If we consider the j spin to be at the center of the spherical sample, the signal generated from its interaction with all other i spins in the sample can be written as an integral over the entire volume:

$$S=|\tfrac{3}{32\pi}M_0t_2\gamma_H\mu_0\times\int_V r^{-3}(3\cos^2\theta-1)\cos\left(\pi\cos\theta\tfrac{r}{d_c}\right)(r^2\sin\theta)\mathrm{d}r\mathrm{d}\theta\mathrm{d}\phi|. \quad [3]$$

Eq.(3) shows that the iZQC signal originating from spin j from its dipolar field interaction with all other spins in the sample depends on r, the internuclear distance between the interacting spins. The dependence of the signal S from r can be factorized as:

$$S = \left| \frac{3}{32\pi} M_0 t_2 \gamma_H \mu_0 \times \sum_r \frac{\pi}{d_c} F\left(\frac{r}{d_c}\right) \right|, \quad [4]$$

where F is defined as:

$$F\left(\frac{r}{d_c}\right) = \frac{d_c}{\pi} \int_{\theta=0}^{\pi} \int_{\phi=0}^{2\pi} r^{-3} \left(3\cos^2\theta - 1\right) \cos\left(\frac{r}{d_c} \pi \cos\theta\right) \left(r^2 \sin\theta\right) d\theta d\phi. \quad [5]$$

Eq.(5) can be easily solved analytically as:

$$F\left(\frac{r}{d_c}\right) = 8\pi \times \frac{3\pi \frac{r}{d_c} \cos\left(\pi \frac{r}{d_c}\right) + \left[\left(\pi \frac{r}{d_c}\right)^2 - 3\right] \sin\left(\pi \frac{r}{d_c}\right)}{\left(\pi \frac{r}{d_c}\right)^4}. \quad [6]$$

The function F, plotted against r/d_c, is shown in Figure 1(d). This function can be essentially regarded as a weighting function for all possible spin-spin interactions that exist in the sample. This weighting function shows that the bulk of the iZQC signal intensity and frequency comes primarily from coherences between spins that are about one correlation distance away. Therefore, in presence of susceptibility gradients, like those created by water-fat interfaces, the iZQC frequency is expected to vary both as a function of sample microstructure and as a function of the selected correlation distance.

To understand how the selection of the correlation distance could affect the water-methylene iZQC frequency, we considered a simple phantom consisting of a fat sphere immersed in water. Specifically, we considered a fat sphere with a diameter of 50 μm and a fat sphere with a diameter of *100 μm*. We then computed the resonance frequency offset generated by the water-fat susceptibility mismatch between the two compartments by using COMSOL Multiphysics (COMSOL, Stockholm, Sweden), assuming an external magnetic field B_0 of 11 T, and a volume susceptibility of −9.04 ppm (2) for the water compartment and −7.79 ppm (37) for the fat compartment. The field offsets generated by the susceptibility mismatch between fat and water for the two phantoms are shown in Figure 2(a) and 2(b).

To compute the resonance frequency of the iZQC signal generated from the interaction of a lipid spin, located at the center of the sphere with frequency ω_f, with all other water spins located outside the sphere, we used the following relation:

$$\omega_{iZQC} = \frac{\omega_f - \left(\sum_{N_j} F\left(\vec{r}_j\right) \omega_w\left(\overrightarrow{r_{\delta i \hat{Z} e}}\right)\right)}{\sum_{N_j} F\left(\vec{r}_j\right)}, \quad [7]$$

where $\omega_w(r_j)$ is the effective water resonance frequency at position r_j, and $F(r_j)$ is the iZQC weighting function defined in Eq.(6). The water-methylene iZQC frequency is computed and plotted in Figure 2(c) for four correlation distances: 25 μm, 50 μm, 100 μm and 200 μm. As one would expect, for a given correlation distance, the iZQC frequency changes with the

microstructure of the sample. More importantly, even for the same phantom, a change of the correlation distance causes a change of the water-methylene iZQC frequency. These dependences are not surprising and are expected for non-mixing spins, like water and fat, which reside in different tissue compartments with different magnetic susceptibilities. On the other hand, this dependence of the iZQC frequency is expected to disappear for homonuclear mixed spin species. If the two homonuclear spins species I and S occupy the same compartments, a change of the correlation distance is expected to change the iZQC linewidth but not its frequency. Without loss of generality, we can understand this concept for a simple homogenous sample with a linear gradient along the z direction (Figure 1(b)). In this case, the susceptibility gradients will introduce a similar frequency offset $\Delta\omega(r_i)$. For a linear gradient, as the correlation distance is increased, the effective frequency difference between the two interactive spins will also increase as $[\omega_I+\Delta\omega(r_i)]-[\omega_S+\Delta\omega(r_j)]$. However, if the spins are completely mixed, for every contribution to the iZQC signal from a pair of I and S spins located at position r_i and r_j, there will be a similar contribution from another pair of I and S spins located at position r_j and r_i whose iZQC frequency will be $[\omega_I+\Delta\omega(r_j)]-[\omega_S+\Delta\omega(r_i)]$. This means that, in general, for homonuclear mixed spins, although the linewidth of the iZQC signal in the presence of microscopic field inhomogeneities may vary as function of the correlation distance, its frequency is expected to remain unchanged.

The situation will be different for a system of mixed heteronuclear spins, where the effect of microscopic field inhomogeneities on the iZQC frequency, though reduced, cannot be completely removed, as the frequency offset $\Delta\omega(r_i)$ produced by the susceptibility gradients will be different for the different nuclei. However, with an appropriate selection of zero and double quantum coherences, the iMQC signal can be made to evolve at $\omega_I-\frac{\gamma_I}{\gamma_S}\omega_S$ in the indirect dimension (25), such that the dependence of the frequency on sample microstructure will be eliminated.

Sequences

Experiments were performed on homonuclear (^{1}H) and heteronuclear (^{1}H and ^{31}P, and ^{1}H and ^{129}Xe) spin systems using the sequences sketched in Figure 3. Specifically, for homonuclear mixed and unmixed spin species a modified version of the CRAZED sequence (13) was used (Figure 3(a)). In this sequence, the iDQC signal that evolves during t_1' is transferred into iZQC during t_1'', and back into iSQC during t_2. The use of a double quantum filter effectively suppresses all spurious signals that are first excited by the second 90° RF pulse.

Experiments on heteronuclear mixed spin systems were performed by using the sequences in Figure 3(b) and 3(c). Sequence 3(b) is the classic heteronuclear CRAZED sequence, in which the iZQC signal evolves during t_1 with a frequency of $\omega_I-\omega_S$. Since the two spins have different gyromagnetic ratios, this sequence is not expected to completely refocus the effect of magnetic field inhomogeneities and therefore, a dependence of the iZQC frequency on the correlation distance is expected in presence of magnetic field inhomogeneities (25).

Sequence 3(c) is a modified version of the inhomogeneity-free heteronuclear sequence originally proposed in (25). In this new sequence, the indirect evolution delays are

incremented such that the signal effectively evolves in the indirect dimension at a frequency of $\omega_I - \frac{\gamma_I}{\gamma_S}\omega_S$.

To provide a brief analysis of this sequence which selects both double quantum (iDQC) and zero quantum coherences (iZQC), we can use the formalism of product operators (38). The first set of 90° RF pulses acts on both channels and excites both spin species onto the transverse plane as double quantum coherences I_-S_-. This operator will evolve under the effect of chemical shift and will also be dephased by the z-gradients such as, at the end of delay t_1', it will have acquired a phase of $I_-S_-e^{i[(\omega_I+\omega_S)t_1'+(\gamma_I+\gamma_S)GTz_i]}$, with z being the z-coordinate of the spins. The second 180° pulse will invert only the S spins, and the double quantum coherences will be transformed into zero quantum coherences: $I_-S_+e^{i[(\omega_I+\omega_S)t_1+(\gamma_I+\gamma_S)GTz]}$. It will then be further dephased by the second gradient pulse, while evolving under chemical shift during the delay t_1'':

$I_-S_-e^{i[(\omega_I+\omega_S)t_1'+(\gamma_I+\gamma_S)GTz]}e^{i[(\omega_I-\omega_S)t_1''+(\gamma_I-\gamma_S)nGTz]}$. The third 90° pulse rotates the S spins back to the z-axis, while flipping I_- spins on the transverse plane into I_+. During the delay t_2, the signal is refocused by the long-range dipolar coupling into:

$I_+e^{i[(\omega_I+\omega_S)t_1'+(\gamma_I+\gamma_S)GTz]}e^{i[(\omega_I-\omega_S)t_1''+(\gamma_I-\gamma_S)nGTz]}e^{-i\omega_I t_2}$. If the condition $(\gamma_I+\gamma_S)GTz + (\gamma_I+\gamma_S)nGTz = 0$ is satisfied, which requires that $n=\frac{\gamma_S+\gamma_I}{\gamma_S-\gamma_I}$, a signal will appear at $t_2=\left(1+\frac{\omega_S}{\omega_I}\right)t_1'+\left(1-\frac{\omega_S}{\omega_I}\right)t_1''$ after the last 90° pulse. By stepping delays t_1' and t_1'' such that $\Delta t_1''=\frac{\gamma_S+\gamma_I}{\gamma_S-\gamma_I}\Delta t_1'$, the signal will effectively evolve in the indirect dimension with a frequency of $\frac{(\omega_I+\omega_S)\Delta t_1'+(\omega_I-\omega_S)\Delta t_1''}{\Delta t_1'+\Delta t_1''}=\frac{(\omega_I+\omega_S)\Delta t_1'+(\omega_I-\omega_S)\frac{\gamma_S+\gamma_I}{\gamma_S-\gamma_l}\Delta t_1'}{\Delta t_1'+\frac{\gamma_S+\gamma_I}{\gamma_S-\gamma_I}\Delta t_1'}=\omega_I-\frac{\gamma_I}{\gamma_S}\omega_S$, while the spectral width along the indirect dimension (F1) will then be $SW=\frac{1}{\Delta t_1'+\Delta t_1''}$.

In Vitro Experiments

All spectroscopic studies were performed on a Varian Inova 500MHz NMR spectrometer (Varian NMR Systems, Palo Alto, CA) using a ^{1}H-^{19}F/^{15}N-^{31}P PFG switchable broadband probe. To evaluate the effect of microscopic susceptibility gradients on the water-methylene iZQC signal, used as probe for MR thermometry, we performed experiments as function of temperature on various samples containing mixtures of water and lipid spins. Two samples consisted of stable homogenous emulsions of corn oil and distilled water with a fat fraction (FF) of 40% and 80%, prepared by following the same procedure described in Bernard et al (39). Another sample was prepared by mixing ovine fat and muscle to achieve, roughly, a 1:1 fat/muscle ratio (WAT/Muscle sample). On the same sample, we also acquired methylene-lipid dissolved xenon (LDX) iDQC/iZQC spectra. The resonance frequency of LDX has a strong temperature dependence of −0.2 ppm/°C (40) and, unlike water, LDX completely mix with lipid protons at the microscopic level. However, in order to detect LDX-methylene iDQC/iZQC signals, high xenon magnetization density had to be reached. This was achieved by charging the sample with thermally polarized xenon gas at high pressure to avoid possible temperature fluctuations from bubbling freshly polarized, cold xenon gas into the sample. For this purpose, the WAT/muscle tissue was placed into a

specially made high-pressure zirconium NMR tube (Daedalus Innovations, Aston, PA), submerged into liquid nitrogen and evacuated. Then, 200 ml of enriched xenon gas (86% ^{129}Xe) was transferred to the NMR tube, which was then sealed and stored at room temperature for at least 24 hours. All scans were performed within two days to minimize chances of the samples separating. Similar experiments could not be made on the emulsion samples as the structure of the emulsion was destroyed during the freeze-thaw cycle needed to dissolve large quantities of xenon in the samples.

All water-methylene iZQC and LDX-methylene iDQC/iZQC experiments were performed as a function of temperature, which was set and maintained by using a temperature controller (L900, Highland Technology, San Francisco, CA). The biopack mode was activated to calibrate the temperature values with an accuracy of 0.1 °C at the beginning of each experiment by using the chemical shift separation between the formyl and methylene protons in a 100% methanol sample. Temperature was set nominally at 25 °C, 32 °C, 39 °C and 45 °C and the samples were allowed to reach equilibrium for one hour before water-methylene iZQC and LDX-methylene iDQC/iZQC spectra were acquired. First and second-order shimming gradients were used to reduce the line widths of both water and fat peaks to acceptable levels.

All water-methylene iZQC spectra were acquired with the methylene peak placed at approximately 400 Hz off resonance, with the following parameters: 4 averages, TR of 8 s, 8192 points and a spectral width of 6000 Hz along the direct dimension (F2). The first 90° pulse and the receiver were phase cycled according to the scheme of (x, y, −x, −y) and (x, −x, x, −x), respectively, to select the desired coherence pathway while suppressing unwanted echoes. The strength of the gradients was varied to select correlation distances of 50 μm, 100 μm and 200 μm. Delay t_1' was stepped 32 times with an increment of 0.2 ms to achieve a spectral width of 5000 Hz along the indirect dimension (F1).

iZQC/iDQC LDX-methylene spectra were acquired by using the sequence in Figure 3(c). For these experiments, the methylene peak was placed roughly at +400 Hz off resonance, while the LDX peak was initially placed at +200 Hz off-resonance, for an effective frequency in the indirect dimension of $\omega_{Xe} - (\gamma_{Xe}/\gamma_H)\omega_H \approx 100$ Hz. Other parameters used were: TR=60 s, 4 averages, $n=\frac{\gamma_H+\gamma_{Xe}}{\gamma_H-\gamma_{Xe}}=1.767$, G = 0.15 $Gauss \cdot cm^{-1} \cdot s$ for a correlation distance of 100 μm, 4096 points in the direct (F2) dimension with a spectral width of 3 kHz. The t_1 and t_2 delays (initial values were 10 ms and 17 ms, respectively) were stepped 24 times by $\Delta t_1' = 0.226\, ms$ and $\Delta t_1'' = \frac{\gamma_H+\gamma_{Xe}}{\gamma_H-\gamma_{Xe}} \times \Delta t_1' = 0.399\, ms$ to obtain an indirect spectral width of 1600 Hz. Single-pulse ^{1}H and ^{129}Xe spectra were also acquired by using a 90°-acquisition scheme on both proton and xenon channels for each temperature value as well at the very end of the experiment, after the temperature was brought back to its original value, to ensure that the emulsions remained stable during the course of the experiment. These spectra were acquired, in both cases, with a total number of points of 8192 and a spectral width of 6 kHz. For post-processing, the proton and xenon peaks in the single pulse spectra were fit with a Voigt function using an in-house MATLAB (MathWorks, Natick, MA) program to extract the resonance frequency information of the methylene, water and lipid-dissolved xenon peaks. Because of the relatively short T2* of the ^{1}H spins in the WAT/

Muscle sample, the resolution of these spectra along the indirect dimension could not be increased without a major loss in spectra SNR. Therefore, to accurately calculate the water-methylene iZQC frequency and the LDX-methylene iDQC/iZQC frequency we measured the phase evolution frequency of the acquired signals as function of the indirect delay, as previously done (35).

Similar experiments were also performed on a sample of phosphoric acids by using the sequences 3(b) to acquire the ^{1}H-^{31}P iZQC spectra, and the sequence 3(c) to acquire the ^{1}H-^{31}P iDQC/iZQC spectra. To select the coherence pathway specified in Figure 3, n was set to 1.47 in 3(b) and 2.36 in 3(c). For the acquisition of iZQC spectra, the ^{31}P and ^{1}H resonances were placed roughly at 200 Hz and 300 Hz off resonance, respectively, leading to a ^{1}H-^{31}P iZQC resonance frequency of (F1, F2)=(ω_P-ω_H,ω_P)=(100 *Hz*,200 *Hz*). For the acquisition of iDQC/iZQC spectra, the ^{31}P and ^{1}H resonances were both placed roughly at 200 *Hz* off resonance such that the iDQC/iZQC resonance was found at (F1, F2)=(ω_P-(γ_P/γ_H)ω_H,ω_P)=(−119 *Hz*,200 *Hz*). In order to resolve changes in resonance linewidth, the resolution of the indirect dimension was set to 2 *Hz* by stepping the t_1 delay in sequence 3(b) by 2 *ms*, while stepping both the t_1' and t_1'' delays in sequence 3(c) by 0.6 *ms* and 1.4 *ms*, respectively. The sample was de-shimmed such that the ^{31}P peak had a symmetric peak shape but varying FWHM of 2 *Hz*, 7 *Hz* and 17 *Hz*. Under the same shimming conditions, spectra were acquired by selecting different correlation distances of 100 μm, 400 μm and 1600 μm.

RESULTS

Figure 4 shows examples of 2D water-methylene iZQC spectra and 2D LDX-methylene iDQC/iZQC spectra acquired by selecting a correlation distance of 100 μm. Because of the coarse resolution used along the F1 dimension (156 *Hz*/px), the temperature shift of the water-methylene peak is barely visible on the water-methylene iZQC spectra, while the temperature shift of the LDX-methylene iDQC/iZQC peak can be clearly seen(b). The water-methylene iZQC frequency, calculated from the signal phase evolution, was (3.462±0.023) ppm, (3.363±0.009) ppm, (3.311±0.010) ppm and (3.251±0.009) ppm for 25.7 °C, 32.8 °C, 40.0 °C and 46.0 °C, respectively, while the LDX-methylene iDQC/iZQC frequency was (2.048±0.019) ppm, (−0.018±0.017) ppm, (−2.370±0.020) ppm and (−3.904±0.022) ppm, for the same temperatures.

Both the water-methylene iZQC and the LDX-methylene iDQC/iZQC frequencies are reported in Figure 5(a) and 5(b), along with the other water-methylene iZQC frequencies obtained from the emulsion phantoms. Water-methylene and LDX-methylene resonance frequency differences as obtained by 1D spectroscopic measurements in the same samples are also reported in the figure. As is clear from Figure 5(a), the water-methylene iZQC resonance frequency differs substantially from the water-methylene frequency separation obtained by 1D spectroscopy, especially for the emulsion phantoms. Also, the difference between these two frequencies is consistently higher when small correlation distances are selected. More interestingly, despite the water-methylene resonance frequency difference as measured from 1D spectra not varying substantially among the 3 samples (the largest variation is of 0.02 ppm between the WAT/muscle and the emulsion samples), the water-

methylene iZQC frequency varied as much as 0.34 ppm, even when the same correlation distance is selected. Even between the 40% emulsion sample and the 80% emulsion sample, the water-methylene iZQC frequency varies as much as 0.02 ppm, whereas the water-methylene separation in the 1D spectra varies by less than 0.008 ppm. Not surprisingly, the water-methylene iZQC frequency difference among the samples is higher for smaller correlation distances, where the difference between the two microstructures differ the most. Not surprising is also the variation of the water-methylene iZQC temperature coefficient, which varies between -0.0101 ppm/°C and −0.0092 ppm/°C between the WAT/muscle and the emulsion samples. The temperature coefficient of the water-methylene iZQC frequency had a variation also as function of the correlation distance of about 2% and 10%, in the 40% and 80% emulsion samples, whereas the variation was 20% in the WAT/muscle sample.

On the contrary, for mixed spins like methylene proton spins and lipid dissolved xenon spins, these variations are not seen. First, the methylene-LDX frequency separation, as calculated from 1D spectra, in ppm with respect to their relative center frequencies, nicely match the methylene-LDX iDQC/iZQC resonance frequency. Second, no variation is seen in the methylene-LDX resonance frequency as function of the correlation distance. This underlines how, for mixed heteronuclear spin systems, the choice of the correlation distance has no effect on their iDQC/iZQC resonance frequency.

Similar results were obtained from the phosphoric acid sample (Figure 6). As expected, the ^{1}H-^{31}P iZQC signal is unable to completely remove the effect of magnetic field inhomogeneities and a dependence of the signal linewidth on shimming conditions and correlation distance is found. A remarkable change of the ^{1}H-^{31}P iZQC frequency is also observed as a function of the correlation distance. On the contrary, the iDQC/iZQC signal is capable of completely removing the effect of magnetic field inhomogeneities, as already pointed out in Branca et al (25), and no variation of the ^{1}H-^{31}P iDQC/iZQC resonance frequency is observed as function of the correlation distance.

DISCUSSION

Magnetic susceptibility gradients are known to negatively affect the accuracy of PRF-based thermometry methods when methylene protons are used as reference (41,42). Here, we investigated how microscopic susceptibility gradients affect the accuracy of water-methylene iZQC-based MR thermometry methods, recently proposed as a way to eliminate the effect of macroscopic field gradients and obtain more accurate temperature information. We found that while the water-methylene iZQC resonance frequency naturally removes magnetic field inhomogeneities at a scale comparable to the correlation distance (32,35), microscopic susceptibility gradients present at a scale comparable to the correlation distance between two immiscible water and fat compartments cannot be removed. On the contrary, we found that, since the effect of these susceptibility gradients is higher at the microscopic scale typically probed by the water-methylene iZQC signal, the water-methylene iZQC frequency presents a strong dependence on sample macrostructure. Specifically, we showed that microscopic susceptibility gradients are not only responsible for a dependence of the iZQC resonance frequency on the correlation distance, but they also produce a variation of the water-methylene iZQC frequency between different samples, much higher than the observed

water-fat resonance frequency variation measured in 1D spectra. This underlines the stronger effect that susceptibility gradients have at the smaller scale probed by the iZQC signal. This variation of the water-methylene iZQC frequency across samples and as a function of the correlation distance, although small and on the order of 0.4 ppm and 0.035 ppm, respectively, can still produce significant temperature inaccuracies, precluding the possibility of performing absolute MR thermometry. This dependence also precludes the possibility for accurate relative temperature measurements in tissues where the water-fat content may change. This is the case in brown adipose tissue, a fatty tissue specialized in non-shivering thermogenesis (43), a process during which tissue lipid content is expected to vary (44).

In this study we also observed a small variation of the water-methylene iZQC temperature coefficient across different samples, consistent with the data reported by others (32). This variation is not surprising since the magnetic susceptibility of fat has a large temperature dependence, which inevitably affects the field offset distribution at the microscopic level probed by the water-methylene iZQC resonance frequency.

It is important to note that this dependence on sample microstructure and the specific choice of correlation distance is an intrinsic characteristic of all iMQC signals originating from spins that do not mix at the microscopic level, and cannot be eliminated by using a different sequence design. Incidentally, this dependence was evident in the data reported by Davis et al (32), where a variation of the water-methylene iZQC frequency on the order of 5% was shown across similar samples of bone marrow, even if a more sophisticated iZQC sequence, the ZQSQ-HOT sequence, was used.

Where the iZQC frequency is expected to deliver on the promise of complete removal of macro and microscopic field gradients is for samples of spins that mix at the molecular level or that are in the same molecule. This is the case, for example, of ^{1}H and ^{31}P spins in phosphoric acids and LDX and methylene protons in fatty tissues. In these cases, however, because the correlated spins have different gyromagnetic ratios, the effect can be completely removed only if the iMQC signal is made to evolve in the indirect dimension at a frequency of $\omega_{Xe} - \frac{\gamma_{Xe}}{\gamma_H}\omega_H$. This possibly opens the door to absolute MR temperature measurements when temperature independent and temperature dependent spins that mix at the microscopic level can be found, as it is the case for methylene protons and LDX spins (40), assuming that the dependence on lipid composition of the LDX frequency is negligible. To this end, when we compared the value of the LDX-methylene iDQC/iZQC frequency found in this study, which equates with the LDX-methylene frequency separation in ppm, to the LDX-methylene frequency separation (40) for similar samples, we can see that the LDX-methylene frequency found here is higher by as much as 12.5 ppm. This discrepancy, however, is the result not of a change in tissue microstructure, but it is the result of the dependence of the LDX frequency on the local xenon concentration. As previously reported, the dependence of the LDX frequency on the in-tissue xenon concentration appears only for in-tissue xenon concentrations that exceed 100 *mM*, well above what can be reached in vivo. In this study, such a high concentration was necessary to create a xenon magnetization density, from thermally polarized xenon spins, high enough to observe these non-linear iMQC signals. The dependence of the xenon resonance frequency on the local xenon density has been studied

already for gaseous xenon and gaseous xenon mixtures (45,46). In gaseous xenon, for example, the virial coefficient of chemical shielding of xenon can be written as:

$$\sigma(\rho,T)=\sigma_0+\sigma_1(T)\rho+\sigma_2(T)\rho^2+\sigma_3(T)\rho^3+\cdots, \quad (7)$$

where σ is the shielding factor of xenon, σ_0, σ_1, σ_2, σ_3 are the zeroth, first, second and third virial coefficients, and ρ is the density of xenon atoms. For xenon dissolved in tissue, like LDX, a similar dependency on the local xenon concentration should be expected. As the in-tissue xenon concentration is increased above a certain threshold, the same intermolecular space is expected to be shared by more than one xenon atom, such that xenon-xenon collisions contribute to the LDX frequency. For gaseous xenon at room temperature, the virial coefficients have been measured to be: σ_1=13.4 *Hz*/amagat, σ_2=0.0039 *Hz*/amagat^2, while σ_3 can be safely ignored at concentrations lower than 150 amagat. If we assume similar virial coefficients for xenon dissolved in lipids, and estimate the in-tissue xenon concentration reached in the WAT/muscle sample in this study, we can estimate the expected increase in the LDX. From a simple SNR comparison between xenon spectra acquired in these studies and previous xenon spectra acquired on similar samples for which the in-tissue concentration was known, the WAT/muscle sample studies here had an estimated xenon concentration of 114 amagat, a concentration that is expected to lead, for gaseous xenon, to an increase in xenon chemical shift of about 12 ppm, very close to the 12.5 ppm shift measured experimentally in our WAT/muscle sample. Such high xenon concentrations cannot be realistically achieved in vivo, where subjects breathe xenon gas at atmospheric pressure. As such, hyperpolarized xenon gas must be used. However, this alone will not guarantee the observation of the LDX-methylene iZQC signal from distal fatty tissues, unless the tissue is highly perfused such that high in-tissue xenon concentrations can be rapidly achieved upon xenon inhalation. This is the case for brown adipose tissue during stimulation of thermogenic activity, during which tissue perfusion is known to increase by several folds (47). In brown adipose tissue, radiation damping effects, which are only generated in the presence of a high magnetization density, have already been observed in vivo from LDX in mice inhaling hyperpolarized xenon gas (48).

The independence of the homonuclear iZQC or heteronuclear iDQC/iZQC frequency on sample structure and correlation distance for mixed spins truly opens the way to absolute MR thermometry, if a couple of temperature-dependent and temperature-independent spins that completely mix at the molecular level can be found. In the meantime, the prospective of using the resonance frequency difference or iDQC/iZQC coherences between temperature-independent methylene protons and lipid dissolved xenon spins to completely remove the effect of microscopic field inhomogeneities while retaining temperature information is appealing and may become possible in the distant future for highly-perfused fatty tissues like brown adipose tissue if highly polarized xenon gas, with a polarization close to unity (49), is made widely available.

CONCLUSIONS

In summary, we have shown that the choice of the correlation distance and the specific distribution of water and fat spins at the microscopic level affect the water-methylene iZQC frequency and its temperature coefficient, undermining the accuracy of MR thermometry methods that use this signal to measure absolute or relative temperature changes. We also showed that these dependencies exist only for spin species that do not mix at the molecular level. For spins that do mix at the molecular level, these signals can help to eliminate macro- and microscopic field inhomogeneities, opening the possibility for true absolute MR thermometry.

Acknowledgments

This work was supported by NIH grant number R01DK108231. We would like to thank Alex Burant for his help with simulation work, and him and Michael Antonacci for proofreading the manuscript.

References

1. McDannold N. Quantitative MRI-based temperature mapping based on the proton resonant frequency shift: Review of validation studies. Int J Hyperth. 2005; 21:533–546. DOI: 10.1080/02656730500096073
2. De Poorter J. Noninvasive MRI thermometry with the proton resonance frequency method: Study of susceptibility effects. Magn Reson Med [Internet]. 1995; 34:359–367. DOI: 10.1002/mrm.1910340313
3. Stollberger R, Ascher PW, Huber D, Renhart W, Radner H, Ebner F. Temperature monitoring of interstitial thermal tissue coagulation using MR phase images. J Magn Reson Imaging. 1998; 8:188–196. DOI: 10.1002/jmri.1880080132 [PubMed: 9500279]
4. Shmatukha AV, Harvey PR, Bakker CJG. Correction of proton resonance frequency shift temperature maps for magnetic field disturbances using fat signal. J Magn Reson Imaging. 2007; 25:579–587. DOI: 10.1002/jmri.20835 [PubMed: 17335067]
5. Mulkern RV, Chung AH, Jolesz Fa, Hynynen K. Temperature monitoring of ultrasonically heated muscle with RARE chemical shift imaging. Med Phys. 1997; 24:1899–1906. DOI: 10.1118/1.598103 [PubMed: 9434972]
6. McDannold N, Barnes AS, Rybicki FJ, Oshio K, Chen N-K, Hynynen K, Mulkern RV. Temperature mapping considerations in the breast with line scan echo planar spectroscopic imaging. Magn Reson Med. 2007; 58:1117–1123. DOI: 10.1002/mrm.21322 [PubMed: 18046702]
7. Sprinkhuizen SM, Bakker CJG, Bartels LW. Absolute MR thermometry using time-domain analysis of multi-gradient-echo magnitude images. Magn Reson Med. 2010; 64:239–248. DOI: 10.1002/mrm.22429 [PubMed: 20577981]
8. Kuroda K. Non-invasive MR thermography using the water proton chemical shift. Int J Hyperth. 2005; 21:547–560. DOI: 10.1080/02656730500204495
9. Ishihara Y, Calderon A, Watanabe H, Okamoto K, Suzuki Y, Kuroda K, Suzuki Y. A precise and fast temperature mapping using water proton chemical shift. Magn Reson Med. 1995; 34:814–823. DOI: 10.1002/mrm.1910340606 [PubMed: 8598808]
10. Cline HE, Hynynen K, Schneider E, Hardy CJ, Maier SE, Watkins RD, Jolesz Fa. Simultaneous magnetic resonance phase and magnitude temperature maps in muscle. Magn Reson Med. 1996; 35:309–315. DOI: 10.1002/mrm.1910350307 [PubMed: 8699941]
11. Hofstetter LW, Yeo DTB, Dixon WT, Kempf JG, Davis CE, Foo TK. Fat-referenced MR thermometry in the breast and prostate using IDEAL. J Magn Reson Imaging [Internet]. 2012; 36:722–732. DOI: 10.1002/jmri.23692

12. Soher BJ, Wyatt C, Reeder SB, MacFall JR. Noninvasive temperature mapping with MRI using chemical shift water-fat separation. Magn Reson Med. 2010; 63:1238–1246. DOI: 10.1002/mrm.22310 [PubMed: 20432295]
13. Vathyam S, Lee S, Warren WS. Homogeneous NMR Spectra in Inhomogeneous Fields. Science (80-). 1996; 272:92–96. DOI: 10.1126/science.272.5258.92
14. Chen S, Huang Y, Sun H, Tan C, Wang K, Cai S. A heteronuclear intermolecular single-quantum coherence scheme for high-resolution 2D J -resolved 1 H NMR spectra in inhomogeneous magnetic fields. Mol Phys. 2016; 114:1520–1527. DOI: 10.1080/00268976.2016.1139205
15. de Graaf RA, Rothman DL, Behar KL. High resolution NMR spectroscopy of rat brain in vivo through indirect zero-quantum-coherence detection. J Magn Reson. 2007; 187:320–326. DOI: 10.1016/j.jmr.2007.06.001 [PubMed: 17587617]
16. Warren W, Richter W, Andreotti A, Farmer B. Generation of impossible cross-peaks between bulk water and biomolecules in solution NMR. Science (80-). 1993; 262:2005–2009. DOI: 10.1126/science.8266096
17. Branca RT, Warren WS. In vivo brown adipose tissue detection and characterization using water-lipid intermolecular zero-quantum coherences. Magn Reson Med. 2011; 65:313–319. DOI: 10.1002/mrm.22622 [PubMed: 20939093]
18. Branca RT, Zhang L, Warren WS, Auerbach E, Khanna A, Degan S, Ugurbil K, Maronpot R. In Vivo Noninvasive Detection of Brown Adipose Tissue through Intermolecular Zero-Quantum MRI. PLoS One [Internet]. 2013; 8:e74206.doi: 10.1371/journal.pone.0074206
19. Warren WS. MR Imaging Contrast Enhancement Based on Intermolecular Zero Quantum Coherences. Science (80-). 1998; 281:247–251. DOI: 10.1126/science.281.5374.247
20. Balla DZ, Faber C. In vivo intermolecular zero-quantum coherence MR spectroscopy in the rat spinal cord at 17.6 T: a feasibility study. Magn Reson Mater Physics, Biol Med. 2007; 20:183–191. DOI: 10.1007/s10334-007-0081-3
21. Mishkovsky M, Eliav U, Navon G, Frydman L. Nearly 10(6)-fold enhancements in intermolecular (1)H double-quantum NMR experiments by nuclear hyperpolarization. J Magn Reson. 2009; 200:142–6. DOI: 10.1016/j.jmr.2009.06.002 [PubMed: 19574073]
22. Tsang A, Stobbe RW, Beaulieu C. In vivo double quantum filtered sodium magnetic resonance imaging of human brain. Magn Reson Med. 2015; 73:497–504. DOI: 10.1002/mrm.25131 [PubMed: 24554463]
23. Rizi RR, Ahn S, Alsop DC, Garrett-Roe S, Mescher M, Richter W, Schnall MD, Leigh JS, Warren WS. Intermolecular zero-quantum coherence imaging of the human brain. Magn Reson Med. 2000; 43:627–632. DOI: 10.1002/(SICI)1522-2594(200005)43:5<627::AID-MRM2>3.0.CO;2-J [PubMed: 10800025]
24. Lin Y-Y, Ahn S, Murali N, Brey W, Bowers CR, Warren WS. High-Resolution, >1 GHz NMR in Unstable Magnetic Fields. Phys Rev Lett. 2000; 85:3732–3735. DOI: 10.1103/PhysRevLett.85.3732 [PubMed: 11030993]
25. Branca RT, Jenista ER, Warren WS. Inhomogeneity-free heteronuclear iMQC. J Magn Reson [Internet]. 2011; 209:347–351. http://dx.doi.org/10.1016/j.jmr.2011.01.018.
26. Faber C, Pracht E, Haase A. Resolution enhancement in in vivo NMR spectroscopy: detection of intermolecular zero-quantum coherences. J Magn Reson. 2003; 161:265–274. DOI: 10.1016/S1090-7807(03)00006-5 [PubMed: 12713979]
27. Chen Z, Cai S, Chen Z, Zhong J. Fast acquisition of high-resolution NMR spectra in inhomogeneous fields via intermolecular double-quantum coherences. J Chem Phys. 2009; 130:84504.doi: 10.1063/1.3076046
28. Lin Y, Chen Z, Cai C, Chen Z. High-resolution NMR spectra under inhomogeneous fields via intermolecular double-quantum coherences. Spectrochim Acta Part A Mol Biomol Spectrosc. 2008; 70:1025–1028. DOI: 10.1016/j.saa.2007.10.022
29. Huang Y, Cai S, Chen X, Chen Z. Intermolecular single-quantum coherence sequences for high-resolution NMR spectra in inhomogeneous fields. J Magn Reson. 2010; 203:100–107. DOI: 10.1016/j.jmr.2009.12.007 [PubMed: 20053574]

30. Lin Y, Gu T, Chen Z, Kennedy S, Jacob M, Zhong J. High-resolution MRS in the presence of field inhomogeneity via intermolecular double-quantum coherences on a 3-T whole-body scanner. Magn Reson Med. 2010; 63:303–311. DOI: 10.1002/mrm.22224 [PubMed: 20099324]
31. Jenista ER, Galiana G, Branca RT, Yarmolenko PS, Stokes AM, Dewhirst MW, Warren WS. Application of mixed spin iMQCs for temperature and chemical-selective imaging. J Magn Reson. 2010; 204:208–218. DOI: 10.1016/j.jmr.2010.02.021 [PubMed: 20303808]
32. Davis RM, Warren WS. Intermolecular zero quantum coherences enable accurate temperature imaging in red bone marrow. Magn Reson Med. 2015; 74:63–70. DOI: 10.1002/mrm.25372
33. Galiana G, Branca RT, Jenista ER, Warren WS. Accurate temperature imaging based on intermolecular coherences in magnetic resonance. Science [Internet]. 2008; 322:421–4. DOI: 10.1126/science.1163242
34. Jenista ER, Branca RT, Warren WS. Absolute temperature imaging using intermolecular multiple quantum MRI. Int J Hyperth. 2010; 26:725–734. DOI: 10.3109/02656736.2010.499527
35. Davis RM, Zhou Z, Chung H, Warren WS. Multi-spin echo spatial encoding provides three-fold improvement of temperature precision during intermolecular zero quantum thermometry. Magn Reson Med. 2016; 75:1958–1966. DOI: 10.1002/mrm.25789 [PubMed: 26077531]
36. Garrett-Roe S, Warren WS. Numerical Studies of Intermolecular Multiple Quantum Coherences: High-Resolution NMR in Inhomogeneous Fields and Contrast Enhancement in MRI. J Magn Reson. 2000; 146:1–13. DOI: 10.1006/jmre.2000.2096 [PubMed: 10968952]
37. Hopkins JA, Wehrli FW. Magnetic susceptibility measurement of insoluble solids by NMR: Magnetic susceptibility of bone. Magn Reson Med. 1997; 37:494–500. DOI: 10.1002/mrm.1910370404 [PubMed: 9094070]
38. Lee S, Richter W, Vathyam S, Warren WS. Quantum treatment of the effects of dipole–dipole interactions in liquid nuclear magnetic resonance. J Chem Phys. 1996; 105:874.doi: 10.1063/1.471968
39. Bernard CP, Liney GP, Manton DJ, Turnbull LW, Langton CM. Comparison of fat quantification methods: a phantom study at 3.0T. J Magn Reson Imaging [Internet]. 2008; 27:192–7. DOI: 10.1002/jmri.21201
40. Zhang L, Burant A, McCallister A, Zhao V, Koshlap KM, Degan S, Antonacci M, Branca RT. Accurate MR thermometry by hyperpolarized 129Xe. Magn Reson Med. 2016; 0:1–10. DOI: 10.1002/mrm.26506
41. Baron P, Deckers R, Bouwman JG, Bakker CJG, de Greef M, Viergever MA, Moonen CTW, Bartels LW. Influence of water and fat heterogeneity on fat-referenced MR thermometry. Magn Reson Med. 2016; 75:1187–1197. DOI: 10.1002/mrm.25727 [PubMed: 25940426]
42. Sprinkhuizen SM, Bakker CJG, Ippel JH, Boelens R, Viergever MA, Bartels LW. Temperature dependence of the magnetic volume susceptibility of human breast fat tissue: an NMR study. Magn Reson Mater Physics, Biol Med. 2012; 25:33–39. DOI: 10.1007/s10334-011-0250-2
43. Cannon B, Nedergaard J. Brown adipose tissue: function and physiological significance. Physiol Rev [Internet]. 2004; 84:277–359. DOI: 10.1152/physrev.00015.2003
44. Stahl V, Maier F, Freitag MT, et al. In vivo assessment of cold stimulation effects on the fat fraction of brown adipose tissue using DIXON MRI. J Magn Reson Imaging. 2017; 45:369–380. DOI: 10.1002/jmri.25364 [PubMed: 27421080]
45. Jameson CJ, Jameson AK, Cohen SM. Temperature and density dependence of 129 Xe chemical shift in xenon gas. J Chem Phys. 1973; 59:4540–4546. DOI: 10.1063/1.1680652
46. Jameson CJ, Jameson AK, Cohen SM. Xe contact shift in oxygen gas. Mol Phys. 1975; 29:1919–1927. DOI: 10.1080/00268977500101671
47. Thurlby PL, Trayhurn P. Regional Blood Flow in Genetically Obese (ob/ob) Mice The Importance of Brown Adipose Tissue to the Reduced Energy Expenditure on Non-Shivering Thermogenesis. Pflugers Arch. 1980; 385:193–201. [PubMed: 7190682]
48. Branca, R., Khanna, A., Freeman, M. 100x Enhancement of Hyperpolarized Xenon-129 Dissolved-phase Signal During Functional MR studies of Fatty Tissues. Miami Beach, Florida, USA: 2012. Experimental Nuclear Magnetic Resonance Conference.

49. Nikolaou P, Coffey AM, Walkup LL, et al. Near-unity nuclear polarization with an open-source 129Xe hyperpolarizer for NMR and MRI. Proc Natl Acad Sci U S A [Internet]. 2013; 110:14150–5. DOI: 10.1073/pnas.1306586110

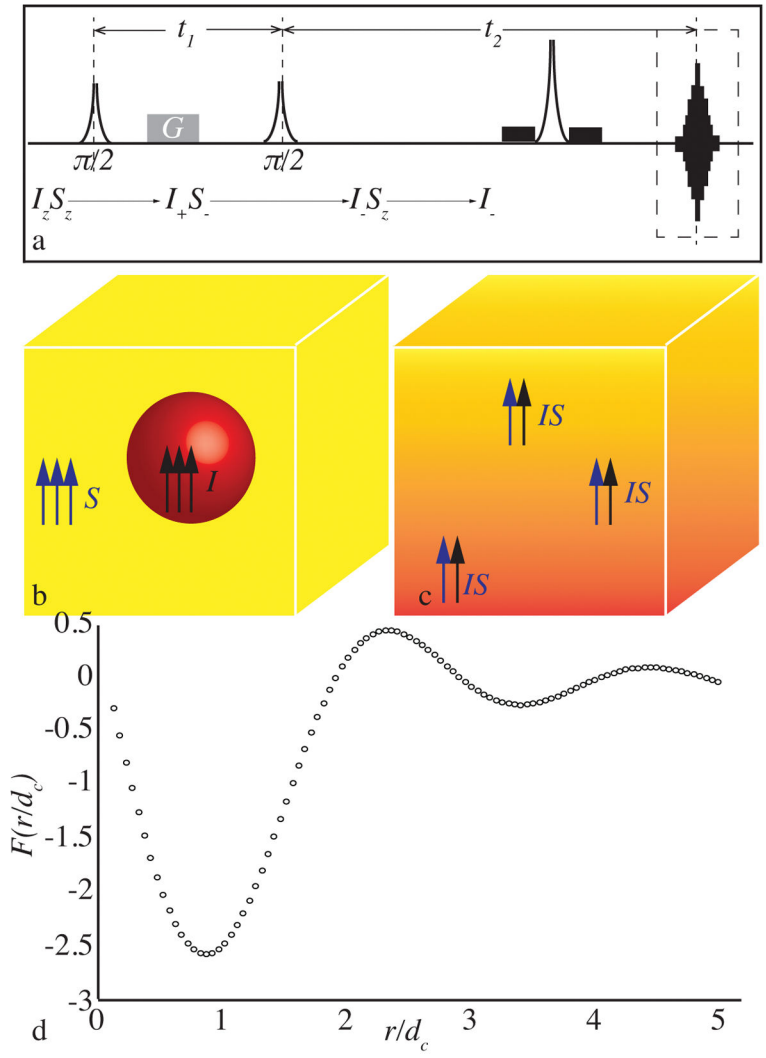

FIG.1.

(a) Original HOMOGENIZED CRAZED sequence. (b) Sketch showing different spin species residing in different compartments. (c) Sketch showing two spin species residing in the same compartments under the effect of an inhomogeneous field. (d) Plot of the $F(r/d_C)$ function, which shows that most of the iZQC signal originates from spins that are about 1 correlation distance away. (1-column)

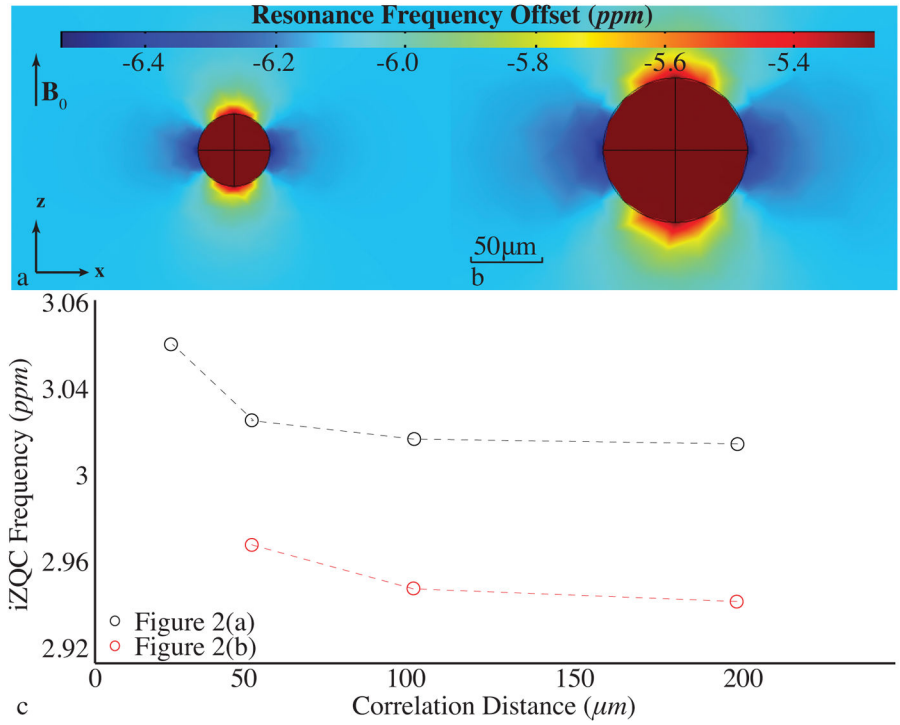

FIG.2.

Effect of microscopic susceptibility differences on the water-methylene iZQC frequency. (a) Frequency offset generated by water and fat susceptibilities for a 50 *μm*-diameter fatty droplet. (b) Frequency offset generated by water and fat susceptibilities for a 100 *μm*-diameter fatty droplet. (c) Computed water-methylene iZQC frequencies (3.5 ppm was the unperturbed frequency difference assumed between methylene and water spins) for the above geometries as function of the correlation distance dc. (1.5-column)

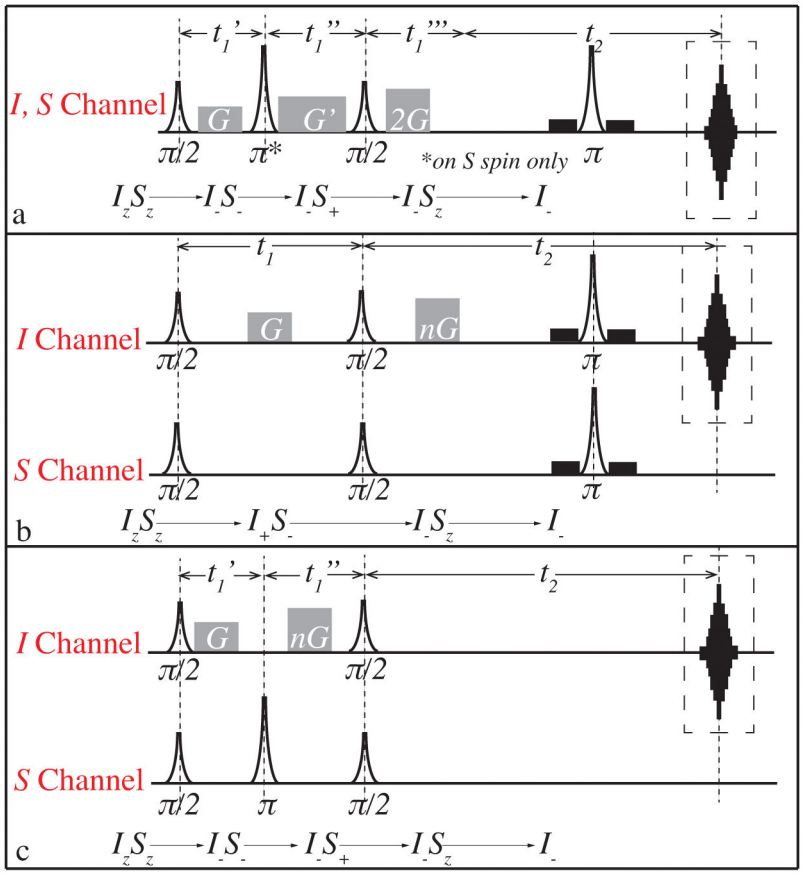

FIG.3.

Sequences used in this study. (a) Modified homonuclear iZQC sequence. (b) Heteronuclear iZQC sequence. (c) Modified version of the inhomogeneity-free iDQC/iZQC sequence proposed in (25). (1-column)

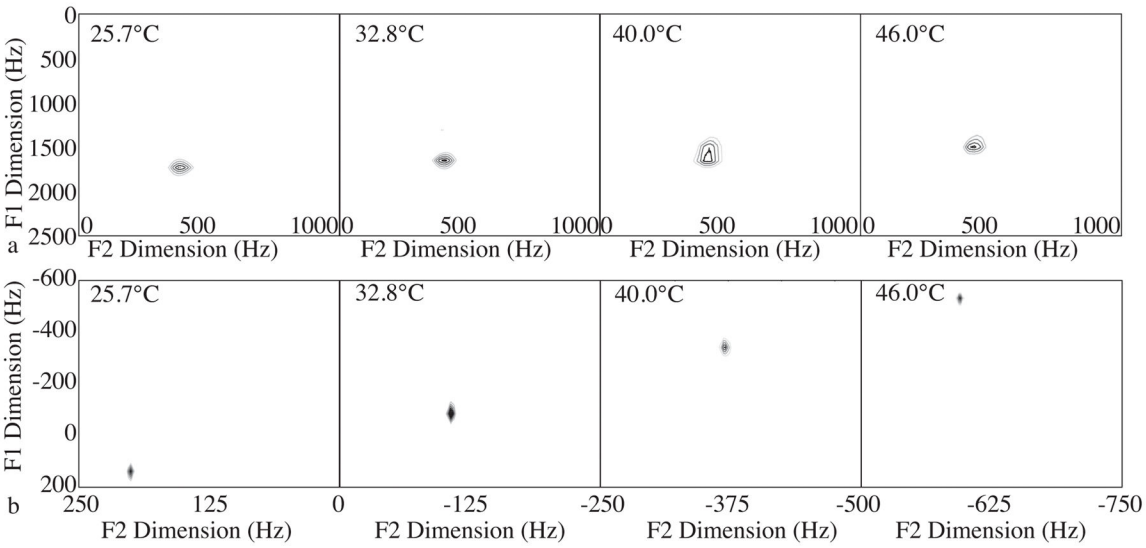

FIG.4.

(a) 2D spectra acquired from the WAT/Muscle sample at four temperatures showing the water-methylene iZQC peak between water and methylene spins. (b) 2D spectra acquired from the WAT/Muscle sample at four temperatures showing the LDX-methylene iDQC/iZQC peak. (2-column)

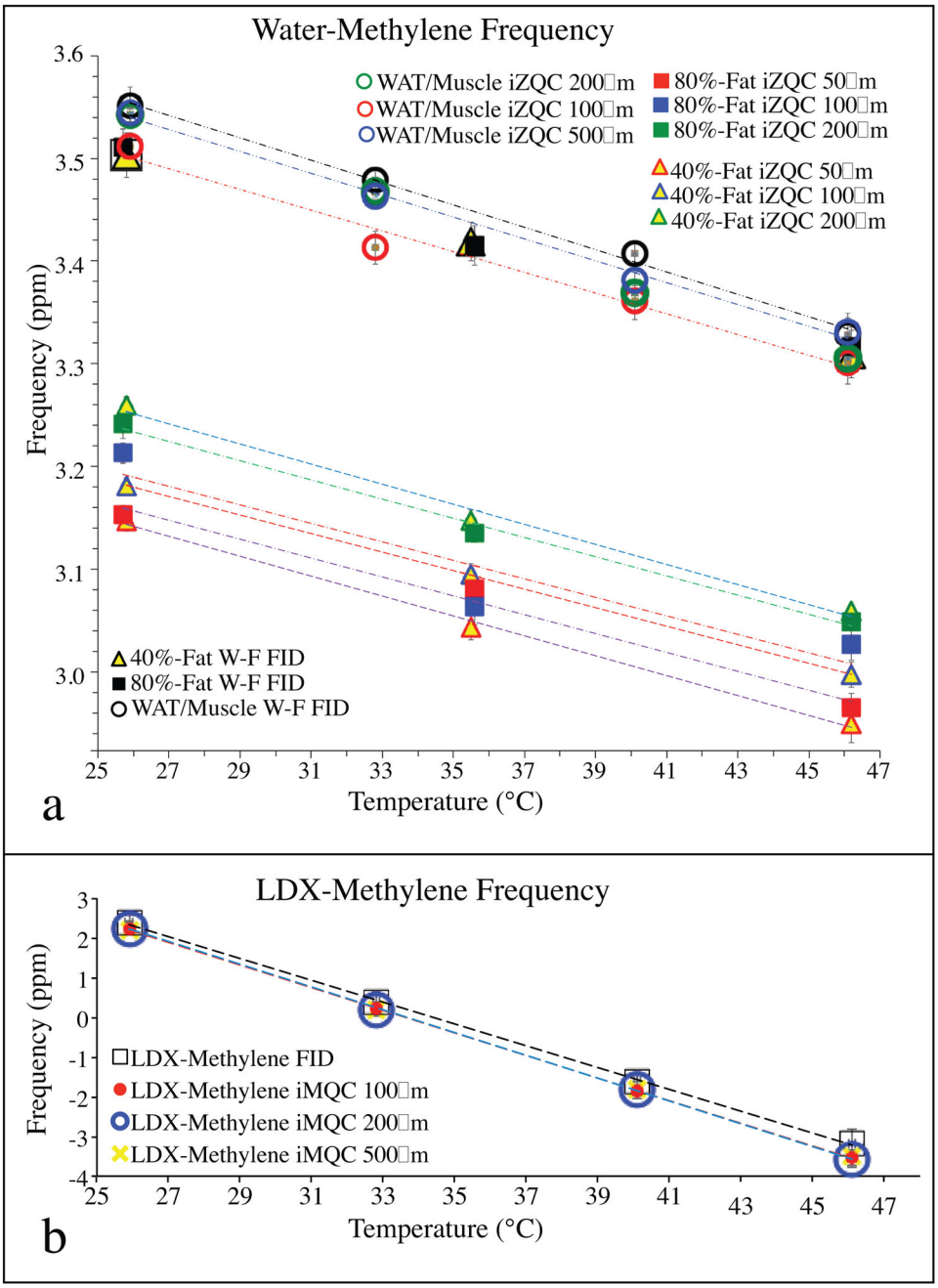

FIG.5.

Dependence of iZQC frequency on correlation distance and temperature by using (a) homonuclear iZQC sequence shown in Figure 3(a) and (b) heteronuclear iZQC sequence shown in Figure 3(c). (2-column)

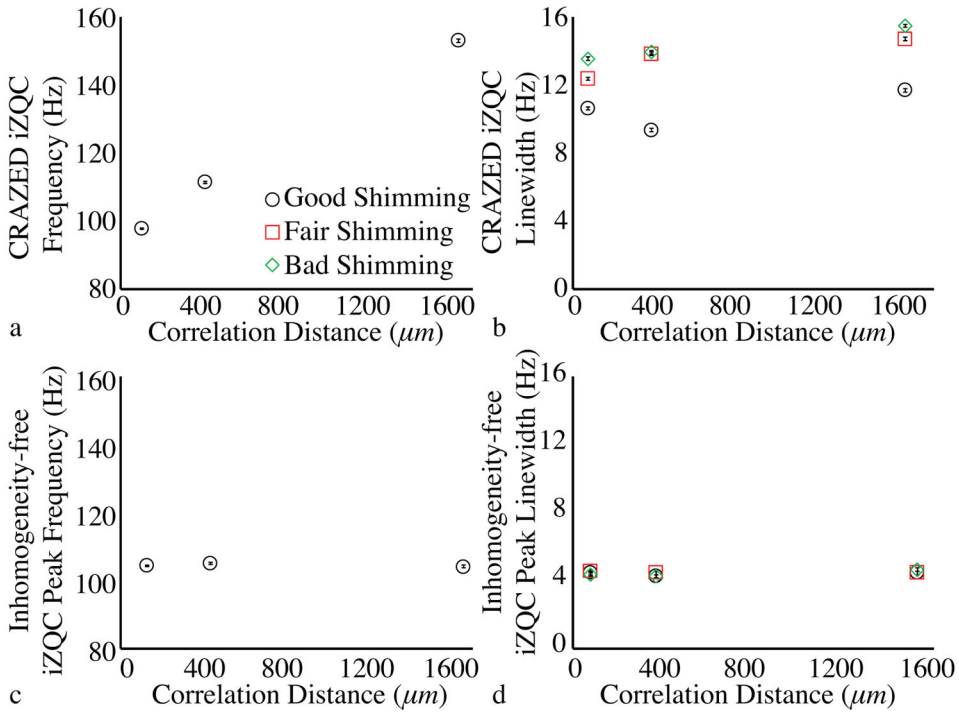

FIG.6.

^{1}H -^{31}P iZQC and iDQC/iZQC resonance frequencies (a–c) and linewidths (b–d) as measured for phosphoric acid as a function of the correlation distance. For a heteronuclear spin system, the iDQC/iZQC resonance frequency is able to completely remove the effect of microscopic field inhomogeneities and therefore eliminate the dependence of its frequency on the choice of the correlation distance. (2-columns)